Front. Mech. Eng. 2022, 17(4): 49
https://doi.org/10.1007/s11465-022-0705-3

RESEARCH ARTICLE

Time of flight improved thermally grown oxide thickness measurement with terahertz spectroscopy

Zhenghao ZHANG[a,b‡], Yi HUANG[a,b‡], Shuncong ZHONG (✉)[a,b], Tingling LIN[a,b], Yujie ZHONG[a,b], Qiuming ZENG[a,b], Walter NSENGIYUMVA[a,b], Yingjie YU[c], Zhike PENG[d]

[a] *Fujian Provincial Key Laboratory of Terahertz Functional Devices and Intelligent Sensing, School of Mechanical Engineering and Automation, Fuzhou University, Fuzhou 350108, China*
[b] *Institute of Precision Instrument and Intelligent Measurement & Control, Fuzhou University, Fuzhou 350108, China*
[c] *School of Mechatronic Engineering and Automation, Shanghai University, Shanghai 200072, China*
[d] *School of Mechanical Engineering, Ningxia University, Yinchuan 750000, China*
✉ *Corresponding author. E-mail: sczhong@fzu.edu.cn (Shuncong ZHONG)*

ABSTRACT As a nondestructive testing technique, terahertz time-domain spectroscopy technology is commonly used to measure the thickness of ceramic coat in thermal barrier coatings (TBCs). However, the invisibility of ceramic/thermally grown oxide (TGO) reflective wave leads to the measurement failure of natural growth TGO whose thickness is below 10 μm in TBCs. To detect and monitor TGO in the emergence stage, a time of flight (TOF) improved TGO thickness measurement method is proposed. A simulative investigation on propagation characteristics of terahertz shows the linear relationship between TGO thickness and phase shift of feature wave. The accurate TOF increment could be acquired from wavelet soft threshold and cross-correlation function with negative effect reduction of environmental noise and system oscillation. Thus, the TGO thickness could be obtained efficiently from the TOF increment of the monitor area with different heating times. The averaged error of 1.61 μm in experimental results demonstrates the highly accurate and robust measurement of the proposed method, making it attractive for condition monitoring and life prediction of TBCs.

KEYWORDS thermal barrier coatings, thermally grown oxide, terahertz spectroscopy, time of flight

1 Introduction

The thermal barrier coating (TBC) is an advanced materials system deposited on the surface of refractory metal or superalloy. With their high-temperature resistance, TBCs can increase the service temperature with an improvement of thermal efficiency, and protect the substrate alloy, thus its application has been increased in the petrochemical, ship, and aerospace industries [1,2]. Normally, a TBC system is structured by a ceramic topcoat and a metallic bondcoat on the alloy substrate. During the service time, the thermally grown oxide (TGO) grows between the ceramic topcoat and the metallic bondcoat when the working temperature is above 700 °C, as performed in Fig. 1 [3]. At first, the TGO film can protect the alloy substrate to reduce oxidation. On the other hand, the thermal oxidation stress induced by the TGO growth is the main cause of performance degradation and failure in TBCs. Especially the crack formation and spalling of TBCs easily occur when the TGO grows to more than 10 μm [4–6]. Therefore, the TGO thickness measurement has a great significance for condition monitoring of TBCs system to ensure the equipment's safety.

Many nondestructive testing techniques have been proposed to detect the TBCs system, including acoustic emission [7], water immersion ultrasonic [8], pulsed and lock-in thermography [9], eddy current testing [10], X-ray [11], and digital image correlation [12]. Besides, Dai et al. [13] proposed a method that combined soft lithography gratings with moiré interferometry to measure Young's modulus of TBC. Lu et al. [14] used Cr^{3+} photoluminescence piezospectroscopy technology to analyze the thermal oxidation stress of TBC, and simulated spectra peaks from the measured spectral data.

Received March 8, 2022; accepted May 6, 2022

‡ These authors contributed equally.

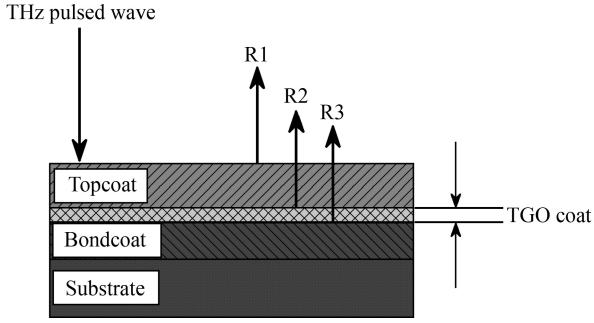

Fig. 1 Typical thermal barrier coating system with thermally grown oxide (TGO).

Shi et al. [15] developed a coupling algorithm based on gray gradient space histogram entropy and sparse representation-based classifier to evaluate the variation of the porosity of TBC. Among these techniques, terahertz time-domain spectroscopy (THz-TDS) had been demonstrated that it has comparable performance in material characterization and damage detection [16–19]. Because it has great abilities for noncontact inspection, high precision, and good penetration for non-metallic materials, some thickness measurement and condition monitoring methods based on THz-TDS technology are developed for material characterization of TBCs and other coatings [20–22]. Zhong et al. [23] obtained the structural information of pharmaceutical tablets by terahertz pulse imaging, and demonstrated it can quantify thicker coatings in the range of 40−140 μm and beyond. Su et al. [24] proposed a THz-TDS-based method to measure the thickness and quality of four layers of car paint on different substrates. Unnikrishnakurup et al. [25] evaluated the degree of degradation of the thin air plasma sprayed TBC topcoat thickness using pulsed thermography and terahertz time-domain spectrum technique, and superiority of terahertz technology was proved. Waddie et al. [26] presented a normal incidence terahertz reflectivity technique to determine the optical thickness and birefringence of yttria-stabilized zirconia (YSZ) TBC. Ye et al. [27] explored a nondestructive porosity evaluation method based on the terahertz time-domain broadening effect.

Caused by the temporal duration limitation of the terahertz pulse, the conventional axial resolution of the general THz-TDS system remains a few tens of microns [28]. Although an attempt to promote the axial resolution used the interferometer has been reported as 17 μm, which is still more than the TGO thickness (usually less than 10 μm) [29]. The propagation time limitation of terahertz pulse, the attenuation of terahertz waveform in ceramic coat, all these factors have resulted in the invisible of TGO characteristic waveform in experimental terahertz signal. Thus, it has difficulties in the application of THz-TDS technology for natural growth TGO measurement. To deal with this problem, some current researches have been combining the neural network method and THz-TDS technique. Ye et al. [30] proposed a novel hybrid artificial neural network combined with the terahertz non-destructive testing technology to predict the thickness of interface delamination in the early stage. Cao et al. [31] investigated a technique that combined THz-TDS and machine learning classifiers to identify discontinuities in TBCs. Luo et al. [32] developed an algorithm that combined the stationary wavelet transform and backpropagation neural network based on terahertz pulse signal to predict the thickness up to 1−29 μm of the TGO. At present, there is a lack of accurately labeled actual experimental signals, the analog signals are commonly used as training samples in the artificial intelligence model of TGO thickness measurement. Due to the deficiency of effective, comprehensive, and sufficient training samples, the detection ability of these models is questioned in the actual growth TGO signals.

In this article, the linear relationship between TGO thickness and time of flight (TOF) change is performed by terahertz propagation characteristic simulation. By deducing the effect of environmental noise and system oscillation in experimental signals, the accurate averaged TOF is acquired by the wavelet soft threshold and cross-correlation. Then TOF increment is calculated by comparing the different TOFs of TBC signals after various heating times, and finally, TGO thickness can be obtained.

This paper is structured as follows: The terahertz pulse wave propagation characteristic simulation in TBC is given in Section 2. In Section 3, the TBC system experimental setup and terahertz pulse signal analysis are presented. A time of flight improved TGO thickness measurement method, calculated results, and discussion are performed in Section 4. Finally, conclusions are given in Section 5.

2 Terahertz pulse wave propagation characteristic simulation

The terahertz wave propagations in TBCs with different thickness TGO are simulated by the XFdtd software through finite difference time domain method to study the influence of thickness change on terahertz signal. The function of Gaussian pulse derivative is selected to be the terahertz incident waveform and pulse width is set to be 2 ps, as shown in Fig. 2. The grid sizes are: $\Delta x = 0.03000$ mm, $\Delta y = 0.03000$ mm, and $\Delta z = 0.00245$ mm, then the time step can be calculated using the formula $\Delta t = \frac{1}{c}\left(\frac{1}{\Delta x^2} + \frac{1}{\Delta y^2} + \frac{1}{\Delta z^2}\right)^{-\frac{1}{2}}$, where c is the light velocity. Thus, the time step is 0.0081165 ps, which is similar to the TeraPulse 4000 system temporal resolution (about 0.0081 ps). The simulated boundary condition is set to be perfectly matched layer absorbing boundary and layer number is 8. Because the materials of both the substrate and bondcoat are the metal that almost reflects the terahertz wave, the types of materials are defined using

the metal materials that come with the software. The material types of TGO coat and ceramic topcoat are defined as the non-dispersive model, and refractive indexes are set to be 5.6 and 2.8 [32].

The thicknesses of alloy substrate, metal bondcoat, and ceramic topcoat are 2000, 200, and 200 μm, and the TGO thicknesses are set to be 10, 20, 30, 40, and 50 μm respectively. Figure 3 shows the propagation waveform of the terahertz incident waveform in TBCs for different thicknesses of the TGO. First, it can be seen that the ceramic/TGO reflective wave can be observed when the TGO thickness is more than or equal to 20 μm. It should be noted that its characteristic waveform is not completely performed due to the TGO thickness cannot support the propagation of one terahertz pulse waveform. Second, associated with the TGO thickness, the TGO/metal bondcoat reflective wave exhibit a phase shift, i.e., the time change of signal point at wave trough. However, the characteristic waveform of TGO is absolutely attenuated since the TGO thickness decreases to 10 μm. Figure 4 plots the terahertz propagation waveform with TGO thickness varies in 0−9 μm. The two reflective waves from the upper and lower surfaces of the TGO would be aliased when the thickness is small enough, making difficulty in thickness identification. It is noted that TGO thickness is less than or equal to 10 μm in the early and middle stages. Therefore, traditional methods via calculating the TOF between ceramic/TGO and TGO/metal reflective waves failed to obtain the TGO thickness. It can be seen that the TOF increases with the growth of TGO thickness in Fig. 5, the fitting curve also performs this pretty linear relationship between TOF and TGO thickness. Thus, the TGO thickness could be expected to be obtained by the accurate calculation of the TOF increment.

3 TBC system experiment and signal analysis

3.1 Experimental setups

A series of experiments are carried out to measure the thickness variation of TGO in TBC after thermal cycling.

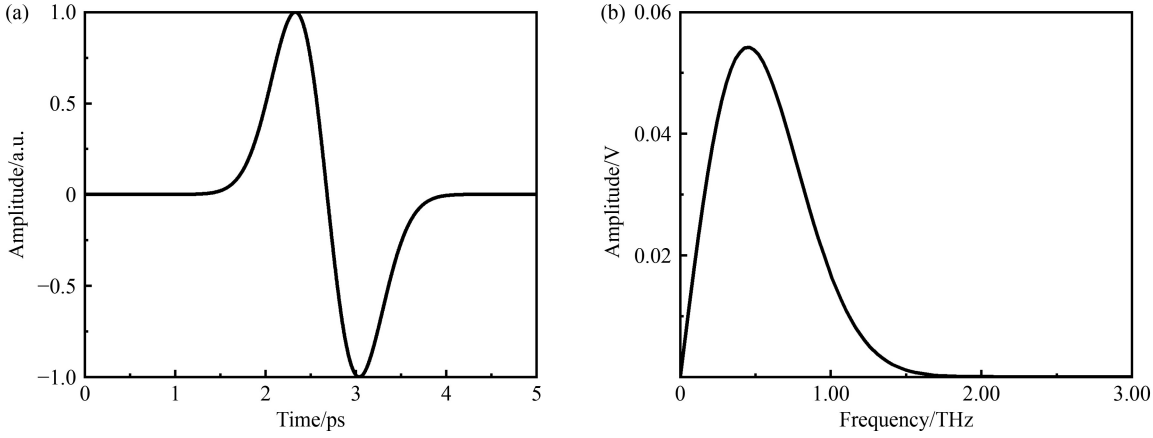

Fig. 2 Terahertz incident signal in simulation: (a) time-domain pulse and (b) its frequency spectrum.

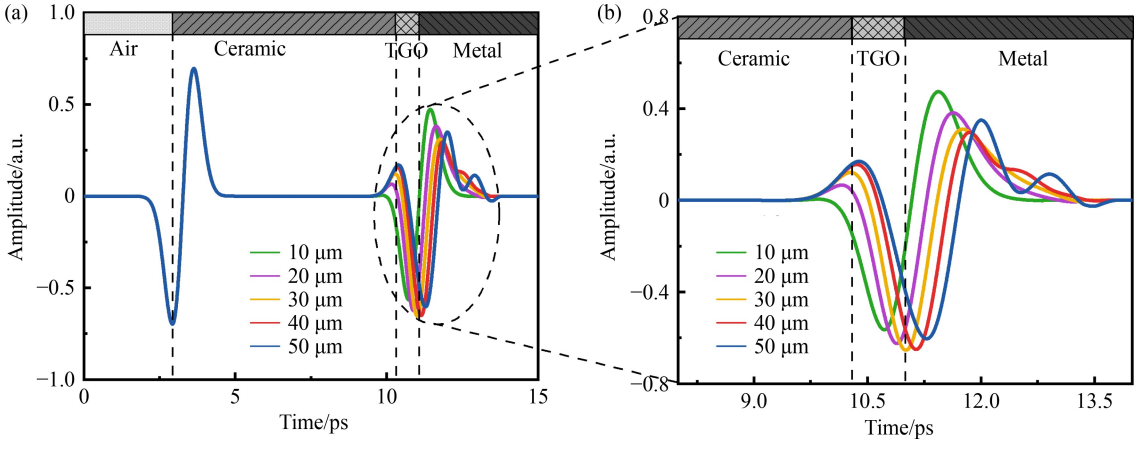

Fig. 3 Terahertz propagation waveform with different thicknesses of the thermally grown oxide (TGO): (a) terahertz propagation waveform and (b) its local waveform.

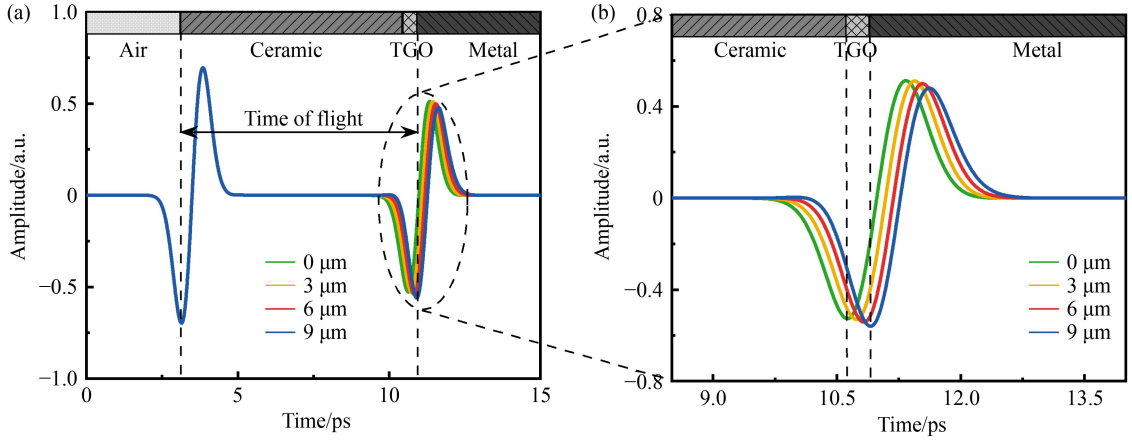

Fig. 4 Terahertz propagation waveform for the actual thickness range of the thermally grown oxide (TGO): (a) terahertz propagation waveform and (b) its local waveform.

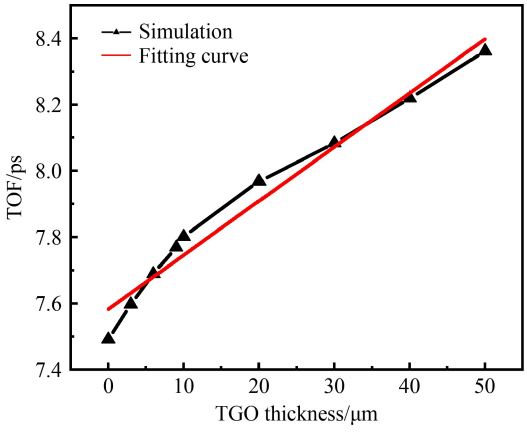

Fig. 5 Linear relationship between the time of flight (TOF) and the thermally grown oxide (TGO) thickness.

In all measurements, we used the terahertz time-domain spectrum and imaging system TeraPulse 4000 (TeraView Ltd., UK), as shown in Fig. 6. The photoconductive antenna is pumped by a femtosecond laser pulse from a laser to generate the terahertz radiation, which is collected, collimated, and focused on the test sample. Then the reflected terahertz pulse is acquired and focused on the terahertz detector. The system also includes a two-dimensional mobile platform that can rapidly move the sample to change the terahertz pulse facula position relative to the sample. Thus, the terahertz pulse can measure each position in the detection area of the sample. The diameter and thickness of substrate are respectively 25 and 3 mm in round TBC sample as Fig. 7(a), which are made by atmospheric plasma spraying from East China University of Science and Technology. It is structured by the common carbon steel substrate, pure Al_2O_3 flame plating coat, and the YSZ topcoat. The Al_2O_3 powders are sprayed on the samples at different times (1, 2, 3, and 4, the thickness of each spray is about 6 μm). The terahertz pulse signals of these samples are performed to explore the relationship of signal changing with TGO thickness, and verify the signal results of software simulation. The dimension of the substrate rectangle TBC sample is 30 mm × 10 mm × 2 mm as Fig. 7(b),

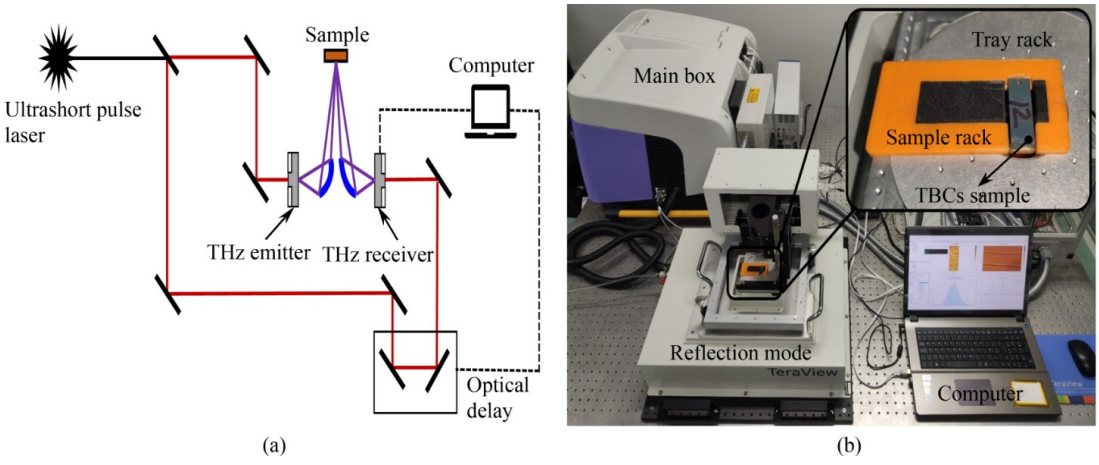

Fig. 6 TeraPulse 4000 system: (a) system structure diagram and (b) actual system.

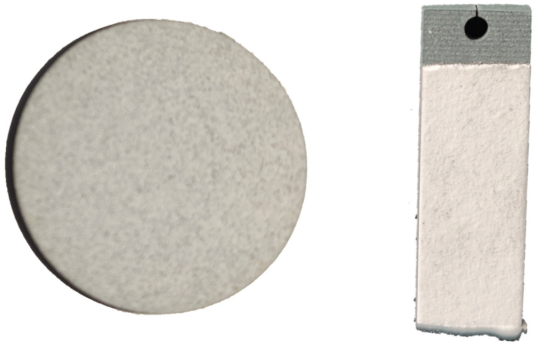

(a) (b)

Fig. 7 Thermal barrier coating samples: (a) round sample and (b) rectangular sample.

which is made by Wuhan University of Technology. The thermal cycling test of TBC is carried out to obtain the natural growth TGO in further experiments. The materials components and chemical elements in each coat are listed in Table 1.

The spraying process parameters include: The equipment is the Multicoat Automatic Thermal Spraying System (Oerlikon Metco Ltd., Switzerland) with the F4 plasma spray gun; the spraying power is 42 kW, the spraying distance is 100 mm, and powder feeding rates are 6% (metal) and 15% (ceramic). After the grinding and polishing, the sample was tested by the scanning electron microscope (SEM) Phenom ProX (Phenom Ltd., the Netherlands). It also integrates an energy dispersive spectrometer, which can be used for energy dispersive analysis at the same time. Before the rectangular sample are heated used the electric furnace, the grinded bottom edge is coated with high-temperature resistant adhesive. To protect the bottom surface from the influence of grinding and polishing at high temperatures and prevent it from cracking, the high-temperature resistant adhesive was coated on the milled sample surface. The high-temperature resistant adhesive is a two-component cementing agent composed of aluminosilicate powder and a modified curing agent (Yikun Glue Ltd., China). Its main components are alumina and silica, the linear expansion coefficient is similar to ceramic, and the maximum operating temperature is 1700 °C. After coating the adhesive, the sample also needs to be heated at 150 °C for 2 h to solidify the adhesive. The electric furnace is the box type experimental furnace SXL-1200C (Shanghai Jvjing Ltd., China), its continuous working temperature is lower than 1150 °C, the recommended fastest heating rate is 10 °C/min, and the temperature control accuracy is 1 °C. In the temperature control process, the electric furnace temperature is first raised from 10 to 1100 °C in 109 min, then the temperature would be kept at 1100 °C for 1200 min, lastly, the sample is taken out and cooled naturally (the cooling time is usually less than 5 min). After the test by TeraPulse 4000 system, the sample bottom is immersed in the hot water to remove the high-temperature resistant adhesive, and further polishing is carried out to obtain the morphology pictures by SEM.

3.2 Terahertz pulse signal analysis

In order to have further insight into the actual relationship between oxide thickness and phase shift of oxide/metal reflective wave, the terahertz propagation waveforms of TBCs with different layer alumina are plotted in Fig. 8. The characteristic waveform of ceramic/alumina is still not observed in the case of four-layer alumina in TBCs. As shown in Fig. 8, the phase right-shift with the increase in layer numbers of alumina. This high relationship provides a possibility for accurate and robust thickness measurement of actual growth TGO in TBCs by calculating the TOF increment, i.e., the phase shift of wave trough in TGO/metal waveform.

The thermal cycle experiment of the rectangular sample is performed to study the terahertz pulse signal influenced by actual TGO growth. The averaged topcoat thickness is measured using the function of distance calibration in the image from the SEM system as Fig. 9. Caused by the influence of the spraying process and ceramic particles, the ceramic coat thicknesses at different positions cannot keep consistent. In particular, it should be noted that the inhomogeneity of thickness and contour would be further performed in the ceramic topcoat and metal bondcoat after the thermal cycle [33]. The measured thickness at one position seems not so reliable and persuasible, thus the averaged thickness of 388.25 μm is used to represent the ceramic topcoat thickness and TGO thickness. The TGO grows around the bondcoat induced by electric furnace heating, the main component of first growth oxide is Al_2O_3, and then (Cr, Al)$_2O_3$ and (Ni, Co) (Cr, Al)$_2O_4$ spinel structure oxides would generate between Al_2O_3 and ceramic topcoat [34]. The composition analysis of some TGO parts is determined by the energy spectrum analysis function from the Phenom ProX system as Fig. 10, and the content of the main elements is shown in Table 2. The main elements of black oxide

Table 1 Materials components and chemical elements of the rectangular sample

Coat	Material	Brand	Formation method	Chemical elements/wt.%
Substrate	Nickel base alloy	DZ125	Directional solidification and wire cutting	Ni 60.00, Co 10.00, Cr 8.90, Al 5.20, W 7.00, Ta 3.80, Mo 2.00, Hf 1.50, Ti 0.90, other 0.70
Bondcoat	Nickel base alloy powder	TSNI05-01	Atomization	Ni 69.60, Cr 24.80, Al 5.00, Y 0.50, Si 0.03, Fe 0.07
Topcoat	YSZ	KF-231	Coprecipitation method	ZrO_2 91.00, Y_2O_3 8.00, Al_2O_3 0.50, Fe_2O_3 0.50

nearest the bondcoat are the oxygen element and aluminum element as points 2, 4, and 6, and the main elements of gray oxide between black oxide and ceramic topcoat are the oxygen element, aluminum element, nickel element, and chromium element as points 1 and 5. The most important thing is that the TGO contour is unsmooth, thus it is not enough to use the one position thickness to represent the whole TGO thickness of TBC. From the SEM picture, the averaged TGO thickness is calculated as 3.11, 4.01, and 4.99 μm after the heating of 20, 40, and 60 h respectively. The TGO grew fastest in the first 20 h, and the growth rate slowed down along with time. Except for the thickness measurement by SEM, the TeraPulse 4000 system scanning function is also used to obtain terahertz time-domain signals of the TBCs sample. The monitor area is set as the area close to the polishing side of the sample, and the dimension is 6.0 mm × 2.0 mm. The scanning step is 0.2 mm, and 600 signals can be acquired from once scanning. In the acquisition process of experimental signals, the water vapor, thermal radiation noise, carrier noise, and system oscillation of two-dimensional mobile platform, all these factors contribute to the complex waveform. The TGO/metal waveform of the experiment is almost buried in the environmental noise, as shown in Fig. 11. The noise, oscillation waveform, and characteristic waveform are generally in the same amplitude range, caused by the serious attenuation of terahertz waves from porous ceramic. Thus, the recognition and location of the characteristic waveform are challenged in the experimental signal. As a result, there is a large error in the TOF calculation using the traditional threshold method.

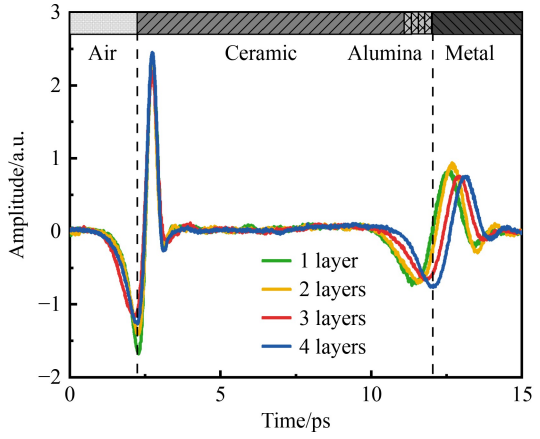

Fig. 8 Terahertz time-domain signals of thermal barrier coatings for different layer alumina.

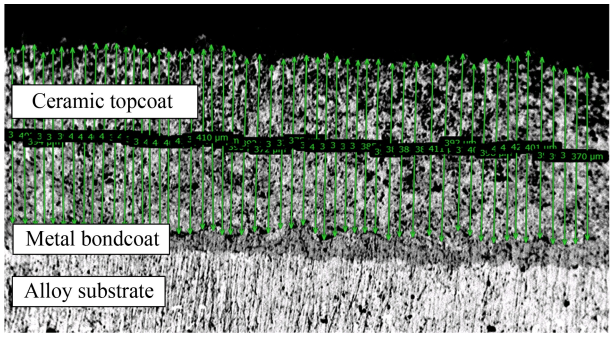

Fig. 9 Scanning electron microscope measurement of ceramic thickness in thermally barrier coatings without thermal cycling.

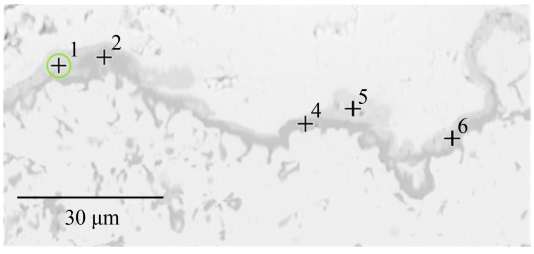

Fig. 10 Thermally grown oxide morphology after 60 h heating times.

Table 2 Main elements content in different parts of thermally grown oxide

Point	Elements content/%			
	O	Al	Ni	Cr
1	34.42	30.08	25.69	9.81
2	37.43	42.12	16.32	4.13
4	35.89	42.50	17.16	4.45
5	30.59	6.50	35.52	27.39
6	32.44	37.63	21.77	8.16

4 Improved TOF calculated method and results

4.1 Improved TOF calculated method

Aiming at the environmental noise and system oscillation

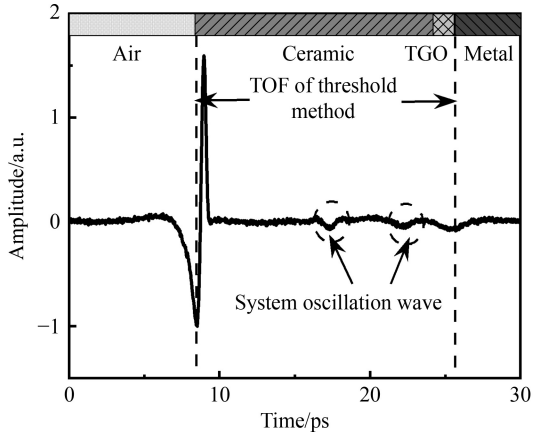

Fig. 11 Terahertz signal interfered by environmental noise and system oscillation. TGO: thermally grown oxide; TOF: time of flight.

wave, the improved TOF calculated method-based wavelet threshold de-noising and cross-correlation is proposed. Assuming the basic wavelet [35] function is ψ, then the function group obtained after stretching and translation is

$$\psi_{a,b}(t)=\frac{1}{\sqrt{|a|}}\psi\left(\frac{t-b}{a}\right), \tag{1}$$

where a is a contraction−expansion factor, b is the translation factor, t is the time in sequence, $a,b\in\mathbf{R}$, and $a\neq 0$.

The continuous wavelet transforms W_f for any function $f(t)\in L^2(\mathbf{R})$ is

$$W_f(a,b)=\langle f,\psi_{a,b}\rangle=\frac{1}{\sqrt{|a|}}\int_{\mathbf{R}} f(t)\psi^*\left(\frac{t-b}{a}\right)\mathrm{d}t, \tag{2}$$

where $*$ denotes conjugation. However, the continuous wavelet transform should be discretized in real-time applications. The discrete divisions of a and b in continuous wavelet transform are set to be $a=a_0^j$ and $b=ka_0^jb_0$, $j\in\mathbf{Z}$, and extended step size $a_0\neq 1$ is a fixture number. a_0 and b_0 are extended step sizes in the discretization process of a and b, respectively, j is the number of discretized values, and k is the discretization coefficient in discretization process. Taken $a_0>1$ and $b_0>1$, the corresponding discrete wavelet function is

$$\psi_{j,k}(t)=a_0^{-j/2}\psi\left(a_0^{-j}t-kb_0\right). \tag{3}$$

Thus, the discrete wavelet function coefficient $w_{j,k}$ of function $f(t)$ is

$$w_{j,k}=\int_{-\infty}^{+\infty} f(t)\psi_{j,k}^*(t)\mathrm{d}t, \tag{4}$$

and its reconstruction formulate is

$$f(t)=\sum_{-\infty}^{+\infty}\sum_{-\infty}^{+\infty} w_{j,k}\psi_{j,k}(t). \tag{5}$$

The noise reduction in measured signals is realized with wavelet transform and threshold set in wavelet threshold de-noising, and its main procedures are: (1) A set of coefficients $w_{j,k}$ is obtained by wavelet transform from noise signal. (2) The proper threshold is selected to threshold processing for wavelet coefficient. The wavelet coefficients whose absolute value is more than the threshold are retained and contracted, and the wavelet coefficients whose absolute value is less than the threshold are set to be 0. (3) The signal after noise removal is obtained by inverse wavelet transform used wavelet coefficients $\hat{w}_{j,k}$.

Due to the characteristic of finite compactly supported orthogonal, the Symlet wavelet has a great performance in the time-domain and frequency domain, and has a pretty linear phase characteristic. Thus sym4 wavelet is set to be the wavelet basis, and the level is 5 [36]. The wavelet coefficients after soft thresholding through adaptive extremum threshold principle, an extreme value λ is generated by the maximin principle

$$\lambda=0.3936+0.1829\log_2 N, \tag{6}$$

where N is the signal length.

The soft threshold function is

$$\hat{w}_{j,k}=\begin{cases}\mathrm{sign}(w_{j,k})\left(|w_{j,k}|-\lambda\right), & \text{when } |w_{j,k}|\geqslant\lambda,\\ 0, & \text{when } |w_{j,k}|<\lambda.\end{cases} \tag{7}$$

The noise reduction via wavelet soft threshold for experimental sample signal is performed as Fig. 12. Since the terahertz signal is interfered with system oscillation wave, some errors produced in wave peak localization and traditional threshold method failed to calculate TOF calculation accurately, thus the cross-correlation is adopted to compute TOF. The similarity of two discrete-time series is estimated through correlation function calculation between the reference signal $f_1(t)$ and experimental signal $f_2(t)$:

$$\begin{cases}f_1(t)=s(t)+sn_1(t),\\ f_2(t)=s(t+\tau_\mathrm{d})+sn_2(t).\end{cases} \tag{8}$$

Supposing the original signal is $s(t)$, the relative time delay of signals is τ_d, $sn_1(t)$ and $sn_2(t)$ are uncorrelated noises, and the cross-correction function $R_{f_1f_2}(\tau)$ is

$$R_{f_1f_2}(\tau)=E\left[f_1(t)f_2(t+\tau)\right]=R_{ss}(\tau-D), \tag{9}$$

where $E[\cdot]$ is the mathematic expectation, $R_{ss}(\cdot)$ is the autocorrelation function of the source signal $s(t)$, τ is the time in correction function, and D is the signal points interval between reference signal and experimental signal in cross-correlation process. The terahertz wave reflected from the smooth metal surface is set to be a reference signal, which is similar to with air/ceramic reflective wave of the experimental signal, and also has a certain similarity with the TGO/metal reflective wave. Therefore, the TOF of corresponding waveforms in the cross-correlation function is taken as the TOF of the experimental signal, as shown in Fig. 13. The average TOFs with different heating times (0, 20, 40, and 60 h) used traditional threshold method are 15.56, 15.93, 16.20, and 16.18 ps, respectively, and the calculated results of the proposed method are 16.19, 16.28, 16.30, and 16.37 ps. Compared with the traditional threshold method, the proposed method can provide more accurate TOFs, and the averages TOFs results decrease by 0.41 ps.

4.2 Thickness calculated results and discussion

For refractive index and topcoat thickness of TBC used reflection measurement, some researchers calculated the coat parameters through transforming the terahertz time-domain signals of different reflective waves into frequency domain signals and calculating [37,38]. However, these methods have the limitations of pretty frequency signal (related to the sample materials), and a high

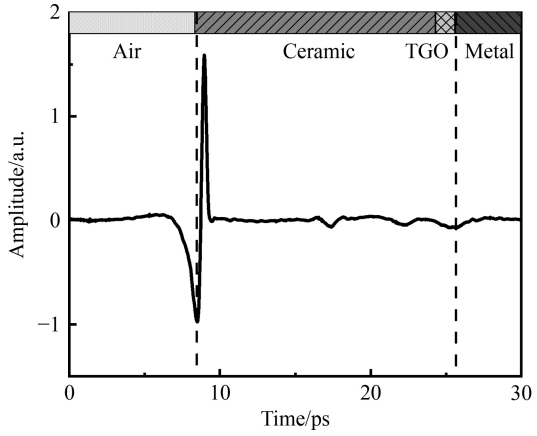

Fig. 12 Denoised terahertz signal used wavelet soft threshold method. TGO: thermally grown oxide.

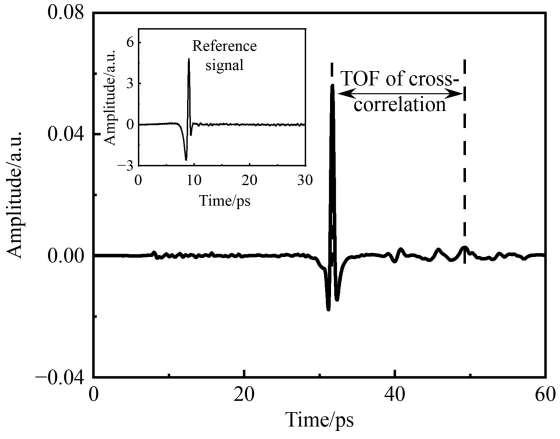

Fig. 13 Cross-correlation function wave between the reference signal and terahertz signal. TOF: time of flight.

requirement of terahertz system acquisition time to obtain the second TGO/metal bondcoat reflective wave. Thus, the common thickness calculation method used reflective terahertz time-domain wave is expressed as [39]

$$d_{\mathrm{c}} = \frac{c\Delta t_1 \cos\theta}{2n_{\mathrm{c}}}, \tag{10}$$

$$n_{\mathrm{a}} \sin\alpha = n_{\mathrm{c}} \sin\theta, \tag{11}$$

where the d_{c} is the ceramic topcoat thickness, Δt_1 is the signal time delay between air/ceramic reflective wave and ceramic/metal reflective wave, α is terahertz incident angle from air into ceramic, n_{c} is the refractive index of ceramic, n_{a} is the refractive index of air, and θ is the terahertz refraction angle. After the TGO growth, the TGO thickness can be computed as

$$d_{\mathrm{T}} = \frac{c(\Delta t_2 - \Delta t_1)\cos\omega}{2n_{\mathrm{T}}}, \tag{12}$$

$$n_{\mathrm{c}} \sin\theta = n_{\mathrm{T}} \sin\omega, \tag{13}$$

where d_{T} is the TGO thickness, Δt_2 is the signal time delay after heating, n_{T} is the TGO refractive index, and ω is the terahertz wave refraction angle from ceramic into TGO.

In the propagation simulation of terahertz pulse signal, the incident angle of terahertz wave is 0, the signal time delay without TGO is 7.47 ps, and the corresponding calculation result of ceramic thickness is 200.07 μm. The recalculated time delay Δt_2 when TBC with TGO is used to compute the TGO thickness used Eq. (3). The calculation results of TGO thickness are 3.12, 6.25, and 9.57 μm, corresponding to the setting value 3.00, 6.00, and 9.00 μm, respectively. Caused by the limitations of grid size and timestep, there are still have some errors even in the simulation results. Some attempts including the smaller grid size and shorter timestep are carried out but the consequent storage space and computing time cannot be accepted, caused by the errors did not decrease much. In TeraPulse 4000 system, the terahertz wave incident angle is 15°. According to Eqs. (1) and (2), the experimental terahertz pulse signals before heating are used to compute the ceramic topcoat refractive indexes, which is 6.25 related to the sample. An assumption that the ceramic topcoat refractive index remains constant during heating is given here. It is widely known that the pure zirconia has a temperature phase transition, as performed in Fig. 14 [40]. The phase transforms from monoclinic to tetragonal at about 1170 °C, and from tetragonal to cubic at about 2370 °C. Although the phase transformation from tetragonal to monoclinic would lead to the 3%–5% volume expansion [41,42]. The addition of 8% Y_2O_3 ingredient can bring the stabilizing of zirconia in high-temperature phase tetragonal, thus the 8YSZ is considered as a TBC material that has the best comprehensive performance and most widely application [43]. Furthermore, the addition of other oxides including Al_2O_3 and Fe_2O_3 resists the phase transition and stabilizes the structure. For convenience, the changes of ceramic refractive index and thickness caused by the thermal cycle are ignored in the next computation.

Some researchers have discussed the optical parameters of Al_2O_3 in the terahertz band. Fattinger and Grischkowsky [44] found that the crystalline Al_2O_3 is birefringent and has a refractive index of $n_0 = 3.07$ for the ordinary ray and $n_{\mathrm{e}} = 3.41$ for the extraordinary ray. On this foundation, Rutz et al. [45] produced the polycrystalline Al_2O_3 which is macroscopically isotropic, and measured the Al_2O_3 value of $n_{\mathrm{A}} = 3.17$. Naturally, the refractive index of natural growth TGO which is a mixed oxide including Al_2O_3 and other spinel oxides should be more than 3.17. However, there have a difficulty in TGO refractive index acquisition caused by the TBC after heating cannot be divided easily. An attempt that the

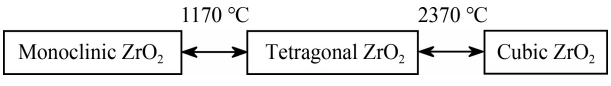

Fig. 14 ZrO_2 phase transition relationship in pure zirconia materials.

sample was immersed in a sulfuric acid solution of 60% solution concentrate for two months is carried out to separate the sample but without any change. The TGO refractive index is temporarily determined as Al_2O_3 value 3.17. Corresponding to the different heating times (20, 40, and 60 h), the TGO calculated results of the traditional threshold method and the proposed method are listed in Table 3. For the traditional threshold method, the maximum error is 26.63 μm and the averaged error is 21.93 μm, which shows that the environmental noise and system oscillation gravely affect the TOF calculation, and lead to a large error in the thickness measurement. By using the presented method, the accurate TGO thicknesses of TBCs after different heating times, are obtained. The maximum error is 2.79 μm and the averaged error is 1.61 μm. Therefore, the proposed TOF improved TGO thickness measurement method for natural growth TGO thickness calculation is accurate and reliable, making it suitable for the condition monitoring and life prediction of the TBCs. It is noted that the TGO thickness error could be further decreased if the TGO refractive index after heating is used. The proposed method is also appropriate for other materials, such as ceramic coatings [30], paint layers [24], drug coatings [46], and composite laminate [19]. The erosion, corrosion, delamination, and other damages widely exist in these layered materials, leading to structural damage and thickness change [17]. The presented method based on THz-TDS has a strong ability to observe the tiny change in the thickness. Therefore, this method is also suitable for damage detection of other layered materials.

5 Conclusions

In summary, a TOF improved TGO thickness measurement method suitable for TBCs condition monitoring had been developed by using the THz-TDS technique. The propagation simulation of terahertz waves in TBCs with different thickness TGO was carried out using the finite difference time domain method. The simulation investigated the phase right-shift of TGO/bondcoat reflective wave due to the TGO growth in the layer boundary of ceramic and bondcoat. Therefore, the TOF increment could calculate the TGO thickness change in the TBCs after the heating cycle and, therefore, facilitate the service life prediction of TBCs. The good agreement of calculative results with setting values verified the efficiency of the proposed method. Experiments for the TBCs with different heating times were also conducted. By reducing the negative effect of environmental noise and system oscillation, the accurate TOF increment was obtained to compute the TGO thickness. Compared with the results from the traditional threshold method, the average error was decreased by 20.32 μm. The experimental results demonstrated that the presented method can accurately and robustly measure the TGO thickness with the advantage of non-destructive and non-contact, making it suitable for thickness measurement of TBCs. The proposed method based on THz-TDS can provide a new tool for damage detection of other layered materials, such as paint layers, drug coatings, and composite laminates. More efforts would be carried out as future work to promote the measurement accuracy, analysis the thermal growth oxidation stress, and predict the crack initiation area in TBCs. The measurement accuracy could be improved by the information acquisition of more optical parameters of ceramic topcoat and TGO after heating. On the other hand, the measurement accuracy also could be elevated by compressing the terahertz pulses width while maintaining the pulse energy. Therefore, its application would be extended in real testing.

Nomenclature

Abbreviations

SEM	Scanning electron microscope
TBC	Thermal barrier coating
TGO	Thermally grown oxide
THz-TDS	Terahertz time-domain spectroscopy
TOF	Time of flight
YSZ	Yttria-stabilized zirconia

Variables

a	Contraction−expansion factor
a_0, b_0	Extended steps in the discretization process of a and b, respectively
b	Translation factor
d_c	Ceramic topcoat thickness
d_T	TGO thickness

Table 3 Calculated results of TGO for different methods

Heating time/h	TGO thickness measured from SEM pictures/μm	TGO thickness measured from THz-TDS using the traditional threshold method/μm		TGO thickness measured from THz-TDS using the proposed method/μm	
		Calculated value	Error	Calculated value	Error
20	3.11	17.73	14.62	3.63	0.52
40	4.01	30.64	26.63	5.53	1.52
60	4.99	29.53	24.54	7.78	2.79

D	Signal points interval between reference signal and experimental signal in corss-correction process
E	Mathematic expectation
$f(t)$	Any function in wavelet transform process
$f_1(t)$	Reference signal
$f_2(t)$	Experimental signal
j	Number of discretized values
k	Discretization coefficient
n_c, n_a	Refractive index of ceramic and air, respectively
n_T	TGO refractive index
N	Signal length
$R_{f_1 f_2}$	Cross-correction function between reference signal and experimental signal
R_{ss}	Autocorrelation function of the source signal
$s(t)$	Original signal without noise
$sn_1(t)$, $sn_2(t)$	Uncorrelated noises in reference signal and experimental signal, respectively
t	Time in the signal sequence
Δt_1	Time delay between air/ceramic reflective wave and ceramic/metal reflective wave
Δt_2	Time delay between terahertz signals before and after TGO growth
$w_{j,k}$	Discrete wavelet function coefficient
W_f	Continuous wavelet transform function
λ	Soft threshold in wavelet function
τ	Time in correction function
τ_d	Relative time delay between reference signal and experimental signal
α	Terahertz incident angle from air into ceramic
θ	Terahertz refractive angle from air into ceramic
ω	Terahertz refractive angle from ceramic into TGO
ψ	Basic wavelet function

Acknowledgements The authors acknowledge the funding they received from the National Natural Science Foundation of China (Grant Nos. 52275096 and 51905102), the Fujian Provincial Science and Technology Project, China (Grant No. 2019I0004), the State Key Laboratory of Mechanical Systems and Vibration, China (Grant No. MSV-2018-07), the Shanghai Natural Sciences Fund, China (Grant No. 18ZR1414200), and the China Postdoctoral Science Foundation (Grant No. 2019M662226).

References

1. Padture N P, Gell M, Jordan E H. Thermal barrier coatings for gas-turbine engine applications. Science, 2002, 296(5566): 280–284
2. Wang L, Di Y L, Liu Y, Wang H D, You H X, Liu T. Effect of TGO on the tensile failure behavior of thermal barrier coatings. Frontiers of Mechanical Engineering, 2019, 14(4): 452–460
3. Deng C, Zheng R G, Wang L, Zhang S Y, Lin X P, Ding K Y. Construction of three-dimensional dynamic growth TGO (thermally grown oxide) model and stress simulation of 8YSZ thermal barrier coating. Ceramics International, 2022, 48(4): 5327–5337
4. Jiang P, Yang L Y, Sun Y L, Li D J, Wang T J. Local residual stress evolution of highly irregular thermally grown oxide layer in thermal barrier coatings. Ceramics International, 2021, 47(8): 10990–10995
5. Evans H E. Oxidation failure of TBC systems: an assessment of mechanisms. Surface and Coatings Technology, 2011, 206(7): 1512–1521
6. Bäker M, Seiler P. A guide to finite element simulations of thermal barrier coatings. Journal of Thermal Spray Technology, 2017, 26(6): 1146–1160
7. bin Zaman S, Hazrati J, de Rooij M, Matthews D, van den Boogaard T. Investigating AlSi coating fracture at high temperatures using acoustic emission sensors. Surface and Coatings Technology, 2021, 423: 127587
8. Wang L, Ding K Y, Lin X P, Li Z, Zheng R G, Yang L W. Defect evolution and microcracks of 8YSZ double-layer thermal barrier coatings by water immersion ultrasound macroscopic detection. Journal of Inorganic Materials, 2019, 34(12): 1265–1271
9. Sharath D, Menaka M, Venkatraman B. Comparison of pulsed and lock-in thermography techniques for debond detection in Ni-B coatings. Materials Evaluation, 2019, 77(12): 1450–1462
10. Wang Z W, Yu Y T. Thickness and conductivity measurement of multilayered electricity-conducting coating by pulsed eddy current technique: experimental investigation. IEEE Transactions on Instrumentation and Measurement, 2019, 68(9): 3166–3172
11. Shen Z Y, Liu Z, Liu G X, He L M, Mu R D, Xu Z H. The morphology, thermal property, and failure mechanism of GdNdZrO thermal barrier coatings by EB-PVD. International Journal of Applied Ceramic Technology, 2021, 18(5): 1623–1629
12. Zhu Q, Zeng Y C, Yang D, Zhu J G, Zhuo L J, Li J, Xie W H. Measurement of the elastic modulus and residual stress of thermal barrier coatings using a digital image correlation technique. Coatings, 2021, 11(2): 245
13. Dai X L, Cao Q K, Xie H M. Characterization for Young's modulus of TBCs using soft lithography gratings and moiré interferometry. Measurement, 2018, 122: 201–211
14. Lu N, Zhang Y H, Qiu W. Comparison and selection of data processing methods for the application of Cr^{3+} photoluminescence piezospectroscopy to thermal barrier coatings. Coatings, 2021, 11(2): 181
15. Shi L C, Long Y, Wang Y Z, Chen X H, Zhao Q F. On-line detection of porosity change of high temperature blade coating for gas turbine. Infrared Physics & Technology, 2020, 110: 103515
16. Ferguson B, Zhang X C. Materials for terahertz science and technology. Nature Materials, 2002, 1(1): 26–33
17. Zhong S C. Progress in terahertz nondestructive testing: a review. Frontiers of Mechanical Engineering, 2019, 14(3): 273–281
18. Nsengiyumva W, Zhong S C, Luo M T, Zhang Q K, Lin J W. Critical insights into the state-of-the-art NDE data fusion techniques for the inspection of structural systems. Structural Control and Health Monitoring, 2022, 29(1): e2857
19. Nsengiyumva W, Zhong S C, Lin J W, Zhang Q K, Zhong J F, Huang Y X. Advances, limitations and prospects of nondestructive

testing and evaluation of thick composites and sandwich structures: a state-of-the-art review. Composite Structures, 2021, 256: 112951

20. Tu W L, Zhong S C, Luo M T, Zhang Q K. Non-destructive evaluation of hidden defects beneath the multilayer organic protective coatings based on terahertz technology. Frontiers in Physics, 2021, 9: 676851
21. Huang Y, Zhong S C, Shen Y C, Yu Y J, Cui D X. Terahertz phase jumps for ultra-sensitive graphene plasmon sensing. Nanoscale, 2018, 10(47): 22466–22473
22. Huang Y, Zhong S C, Shi T T, Shen Y C, Cui D X. Terahertz plasmonic phase-jump manipulator for liquid sensing. Nanophotonics, 2020, 9(9): 3011–3021
23. Zhong S C, Shen Y C, Ho L, May R K, Zeitler J A, Evans M, Taday P F, Pepper M, Rades T, Gordon K C, Müller R, Kleinebudde P. Non-destructive quantification of pharmaceutical tablet coatings using terahertz pulsed imaging and optical coherence tomography. Optics and Lasers in Engineering, 2011, 49(3): 361–365
24. Su K, Shen Y C, Zeitler J A. Terahertz sensor for non-contact thickness and quality measurement of automobile paints of varying complexity. IEEE Transactions on Terahertz Science and Technology, 2014, 4(4): 432–439
25. Unnikrishnakurup S, Dash J, Ray S, Pesala B, Balasubramaniam K. Nondestructive evaluation of thermal barrier coating thickness degradation using pulsed IR thermography and THz-TDS measurements: a comparative study. NDT & E International, 2020, 116: 102367
26. Waddie A J, Schemmel P J, Chalk C, Isern L, Nicholls J R, Moore A J. Terahertz optical thickness and birefringence measurement for thermal barrier coating defect location. Optics Express, 2020, 28(21): 31535–31552
27. Ye D D, Wang W Z, Zhou H T, Huang J B , Wu W C, Gong H H, Li Z. *In-situ* evaluation of porosity in thermal barrier coatings based on the broadening of terahertz time-domain pulses: simulation and experimental investigations. Optics Express, 2019, 27(20): 28150–28165
28. Mitrofanov O, Brener I, Harel R, Wynn J D, Pfeiffer L N, West K W, Federici J. Terahertz near-field microscopy based on a collection mode detector. Applied Physics Letters, 2000, 77(22): 3496–3498
29. Kolpatzeck K, Liu X, Häring L, Balzer J C, Czylwik A. Ultra-high repetition rate terahertz time-domain spectroscopy for micrometer layer thickness measurement. Sensors, 2021, 21(16): 5389
30. Ye D D, Wang W Z, Yin C D, Xu Z, Fang H J, Huang J B, Li Y J. Nondestructive evaluation of thermal barrier coatings interface delamination using terahertz technique combined with SWT-PCA-GA-BP algorithm. Coatings, 2020, 10(9): 859
31. Cao B H, Cai E Z, Fan M B. NDE of dtiscontinuities in hermal barrier coatings with terahertz time-domain spectroscopy and machine learning classifiers. Materials Evaluation, 2021, 79(2): 125–135
32. Luo M T, Zhong S C, Yao L G, Tu W L, Nsengiyumva W, Chen W Q. Thin thermally grown oxide thickness detection in thermal barrier coatings based on SWT-BP neural network algorithm and terahertz technology. Applied Optics, 2020, 59(13): 4097–4104
33. Wei Z Y, Cai H N. Understanding the failure mechanism of thermal barrier coatings considering the local bulge at the interface between YSZ ceramic and bond layer. Materials, 2021, 15(1): 275
34. Yan J R, Wang X, Chen K Y, Lee K N. Sintering modeling of thermal barrier coatings at elevated temperatures: a review of recent advances. Coatings, 2021, 11(10): 1214
35. Daubechies I. The wavelet transform,time-frequency localization and signal analysis. IEEE Transactions on Information Theory, 1990, 36(5): 961–1005
36. Chen X F, Wang S B, Qiao B J, Chen Q. Basic research on machinery fault diagnostics: past, present, and future trends. Frontiers of Mechanical Engineering, 2018, 13(2): 264–291
37. Fukuchi T, Fuse N, Okada M, Fujii T, Mizuno M, Fukunaga K. Measurement of refractive index and thickness of topcoat of thermal barrier coating by reflection measurement of terahertz waves. Electronics and Communications in Japan, 2013, 96(12): 37–45
38. Ye D D, Wang W Z, Zhou H T, Li Y J, Fang H J, Huang J B, Gong H H, Li Z. Quantitative determination of porosity in thermal barrier coatings using terahertz reflectance spectrum: case study of atmospheric-plasma-sprayed YSZ coatings. IEEE Transactions on Terahertz Science and Technology, 2020, 10(4): 383–390
39. Pickwell E, Wallace V P, Cole B E, Ali S, Longbottom C, Lynch R J M, Pepper M. A comparison of terahertz pulsed imaging with transmission microradiography for depth measurement of enamel demineralisation *in vitro*. Caries Research, 2007, 41: 49–55
40. Roncallo G, Barbareschi E, Cacciamani G, Vacchieri E. Effect of cooling rate on phase transformation in 6-8 wt.% YSZ APS TBCs. Surface and Coatings Technology, 2021, 412: 127071
41. Loganathan A, Gandhi A S. Effect of phase transformations on the fracture toughness of *t*′ yttria stabilized zirconia. Materials Science and Engineering: A, 2012, 556: 927–935
42. Ling Y Q, Li Q N, Zheng H W, Omran M, Gao L, Chen J, Chen G. Optimisation on the stability of CaO-doped partially stabilised zirconia by microwave heating. Ceramics International, 2021, 47(6): 8067–8074
43. Cao X Q, Vassen R, Stoever D. Ceramic materials for thermal barrier coatings. Journal of the European Ceramic Society, 2004, 24(1): 1–10
44. Bolivar P H, Brucherseifer M, Rivas J G, Gonzalo R, Ederra I, Reynolds A L, Holker M, de Maagt P. Measurement of the dielectric constant and loss tangent of high dielectric-constant materials at terahertz frequencies. IEEE Transactions on Microwave Theory and Techniques, 2003, 51(4): 1062–1066
45. Rutz F, Koch M, Micele L, de Portu G. Ceramic dielectric mirrors for the terahertz range. Applied Optics, 2006, 45(31): 8070–8073
46. Shen Y C, Taday P F. Development and application of terahertz pulsed imaging for nondestructive inspection of pharmaceutical tablet. IEEE Journal of Selected Topics in Quantum Electronics, 2008, 14(2): 407–415